THE JOURNAL OF BIOLOGICAL CHEMISTRY VOL. 287, NO. 4, pp. 2296–2307, January 20, 2012

Photoaffinity Labeling of Nicotinic Acid Adenine Dinucleotide Phosphate (NAADP) Targets in Mammalian Cells*◆

Received for publication, September 23, 2011, and in revised form, November 15, 2011 Published, JBC Papers in Press, November 23, 2011, DOI 10.1074/jbc.M111.305813

Yaping Lin-Moshier[‡1], Timothy F. Walseth[‡], Dev Churamani[§], Sean M. Davidson[¶], James T. Slama[‖], Robert Hooper[§2], Eugen Brailoiu[**], Sandip Patel[§], and Jonathan S. Marchant[‡3]

*From the [‡]Department of Pharmacology, University of Minnesota Medical School, Minneapolis, Minnesota 55455, the [§]Department of Cell and Developmental Biology, University College London, London WC1E 6BT, United Kingdom, the [¶]Department of Medicine, the Hatter Cardiovascular Institute, University College London, London WC1E 6HX, United Kingdom, the [‖]Department of Medicinal and Biological Chemistry, University of Toledo, Toledo, Ohio 43614, and the **Department of Pharmacology, Temple University School of Medicine, Philadelphia, Pennsylvania 19140*

Background: Nicotinic acid adenine dinucleotide phosphate (NAADP) activates two-pore channels (TPCs) to release Ca^{2+} from intracellular acidic Ca^{2+} stores.
Results: A photoactivatable probe based on NAADP labels proteins distinct from TPCs.
Conclusion: NAADP may bind to an accessory protein within a larger TPC complex.
Significance: First evidence that TPCs act as NAADP-activated Ca^{2+} release channels, but not NAADP receptors.

Nicotinic acid adenine dinucleotide phosphate (NAADP) is an agonist-generated second messenger that releases Ca^{2+} from intracellular acidic Ca^{2+} stores. Recent evidence has identified the two-pore channels (TPCs) within the endolysosomal system as NAADP-regulated Ca^{2+} channels that release organellar Ca^{2+} in response to NAADP. However, little is known about the mechanism coupling NAADP binding to calcium release. To identify the NAADP binding site, we employed a photoaffinity labeling method using a radioactive photoprobe based on 5-azido-NAADP ([^{32}P-5N_3]NAADP) that exhibits high affinity binding to NAADP receptors. In several systems that are widely used for studying NAADP-evoked Ca^{2+} signaling, including sea urchin eggs, human cell lines (HEK293, SKBR3), and mouse pancreas, 5N_3-NAADP selectively labeled low molecular weight sites that exhibited the diagnostic pharmacology of NAADP-sensitive Ca^{2+} release. Surprisingly, we were unable to demonstrate labeling of endogenous, or overexpressed, TPCs. Furthermore, labeling of high affinity NAADP binding sites was preserved in pancreatic samples from TPC1 and TPC2 knockout mice. These photolabeling data suggest that an accessory component within a larger TPC complex is responsible for binding NAADP that is unique from the core channel itself. This observation necessitates critical evaluation of current models of NAADP-triggered activation of the TPC family.

NAADP[4] is a potent Ca^{2+}-releasing messenger that has been shown to regulate many physiological processes encompassing fertilization, secretion, neurite outgrowth, and synaptic function (1–4). Although molecular identification of the Ca^{2+} channel(s) targeted by NAADP remained frustratingly elusive for many years, several lines of evidence have recently unmasked the two-pore channel (TPC) family of endolysosomal proteins as candidate NAADP receptors (5–7). Supporting evidence derives from gain- and loss-of-function approaches, electrophysiological analyses, and radioligand binding. For example, overexpression of either of the two human TPC isoforms (TPC1 and TPC2) enhanced NAADP-evoked Ca^{2+} responses when assessed by Ca^{2+} imaging in multiple cell lines (5–10). Reciprocally, knockdown of endogenous TPC1 ablated NAADP responsiveness (7), and NAADP-activated Ca^{2+} currents were abolished in pancreatic β-cells isolated from a TPC2 knock-out mouse (5). Electrophysiological insight has been derived from different approaches in which TPC activity was recorded from individual lysosomes *in vitro* (11), reconstituted channels in planar lipid bilayers (12), or channels rerouted to the cell surface via mutagenesis of a lysosomal targeting sequence (9, 13). Each approach demonstrated that the addition of NAADP at nanomolar concentrations stimulated Ca^{2+}-permeable currents and/or single channel activity. Finally, radioligand binding methods using membranes overexpressing TPC2 or endogenous TPC isoforms immunoprecipitated from sea urchin eggs demonstrated enhanced [^{32}P]NAADP binding relative to control samples (5, 14). Cumulatively, this growing dataset has established TPCs as NAADP-sensitive Ca^{2+} channels within the endolysosomal system.

* This work was supported, in whole or in part, by National Institutes of Health Grants GM088790 (to J. S. M.) and HL90804 (to E. B.). This work was also supported by Biotechnology and Biological Sciences Research Council (BBSRC) Grant BB/G013721/1 (to S. P.).
◆ This article was selected as a Paper of the Week.
[1] Supported by a doctoral dissertation fellowship from the University of Minnesota Graduate School.
[2] Supported by a BBSRC Ph. D. studentship.
[3] To whom correspondence should be addressed: 6-120 Jackson Hall, 321 Church St. SE, Minneapolis, MN 55455. E-mail: march029@umn.edu.

[4] The abbreviations used are: NAADP, nicotinic acid adenine dinucleotide phosphate; 5N_3-NAADP, 5-azido-NAADP; NAAD, nicotinic acid adenine dinucleotide; TPC, two-pore channel; WCL, whole cell lysate; PAL, photoaffinity labeling; ER, endoplasmic reticulum; Bis-Tris, 2-(bis(2-hydroxyethyl)-amino)-2-(hydroxymethyl)propane-1,3-diol; S, supernatant; P, pellet.

Despite this progress, little is currently known about the structural basis of NAADP interaction with the TPC protein, and the binding site(s) for the endogenous ligand remain unresolved.

PAL methods have proven a useful tool for pharmacological research with utility for first identifying targets of labeled ligands and thereafter for probing the structural basis of drug-receptor interactions (15). Photoactive probes can be generated by simple modification of native ligands to incorporate photoactivatable groups, such as azides, diazirines, diazocarbonyls, or benzophenones (16), or by coupling the native ligand in its entirety to a more generic photoaffinity labeling module (17). The former strategy maximizes the likelihood that the derivatized probe mimics the native ligand properties, whereas the latter approach provides further customizability through exploitation of additional tags to facilitate identification and further purification. In the context of NAADP signaling, recent structure-activity investigations have shown that the 5-position of the nicotinic ring of NAADP is tolerant to substitution (18). Therefore, incorporation of an azide group at this position ($5N_3$-NAADP) provides a simple strategy for derivatization of a photoactivatable NAADP probe (18). Such azido-based photoaffinity probes have previously been successfully applied to study interactions between agonists and different ion channels (19–21). Here, we utilized the [^{32}P-$5N_3$]-NAADP photolabeling strategy with the aim of performing an unbiased characterization of NAADP binding partners within mammalian cells. Although $5N_3$-NAADP recapitulated the essential properties of NAADP as a Ca^{2+}-mobilizing messenger, we were surprisingly unable to demonstrate direct labeling of either endogenous or overexpressed TPC proteins in several mammalian systems or in the sea urchin egg homogenate preparation widely used for studying NAADP-evoked Ca^{2+} signaling. Consequently, we discuss the possibility that accessory components within a larger TPC complex may be responsible for binding NAADP rather than the TPC protein itself.

EXPERIMENTAL PROCEDURES

Chemicals and Reagents—NAADP was synthesized by incubating nicotinamide adenine dinucleotide phosphate (NADP, Sigma-Aldrich) with nicotinic acid in the presence of recombinant *Aplysia* ADP ribosyl cyclase (22) followed by high-performance liquid chromatography (HPLC) purification. Concentrations of NADP and NAADP were estimated using established methods (22). [^{32}P]NAADP and [^{32}P-$5N_3$]NAADP were prepared from [^{32}P]nicotinamide adenine dinucleotide ([^{32}P]NAD, 800 Ci/mmol, PerkinElmer Life Sciences) using methods described elsewhere (23). NADP was freshly purified by HPLC prior to experimentation to remove contaminating NAADP. Construction of TPC vectors tagged with GFP or Myc has been described previously (7, 13). LAMP1-RFP (lysosomal-associated membrane protein-1 in complex with red fluorescent protein) was purchased from Addgene, and pCMV/Myc/ER/GFP (pShooter-ER) was from Invitrogen.

Binding and Ca^{2+} Release Assays—Sea urchin (*Lytechinus pictus*) egg homogenates (50% v/v) were prepared using standard methods (24). Homogenates were diluted in intracellular-like medium (20 mM HEPES, 250 mM potassium gluconate, 250 mM *N*-methyl D-glucamine, 1 mM $MgCl_2$, pH 7.2) to 5% (v/v) for the radioligand binding assay. Homogenates were incubated with [^{32}P]NAADP or [^{32}P-$5N_3$]NAADP (3–7 nM) supplemented with the indicated concentrations of unlabeled NAADP (90 min on ice). Binding reactions (100 μl) were terminated by dilution with 1 ml of HEPES buffer followed by centrifugation (21,000 $\times$ *g* for 30 min, 4 °C). Following aspiration of supernatant, pellets were washed, and radioactivity was determined by liquid scintillation counting.

For the sea urchin Ca^{2+} release assay, homogenates were diluted to 2.5% (v/v) with intracellular-like medium supplemented with an ATP regeneration system (1 mM MgATP, 10 mM creatine phosphate, 10 units/ml creatine phosphokinase) and 3 μM fluo-3 for fluorometric detection of free Ca^{2+}, as described previously (25). Calcium imaging and microinjection of SKBR3 cells were performed using methods described in Ref. 7.

Sample Preparation—SKBR3 (human breast carcinoma) and HEK293 (human embryonic kidney) cells were from ATCC. SKBR3 cells were cultured in McCoy's 5A medium, and HEK293 cells were cultured in minimal essential medium. All media were supplemented with 10% fetal bovine serum (FBS), penicillin (100 units/ml), streptomycin (100 μg/ml), and L-glutamine (290 μg/ml) (Invitrogen). Whole cell lysate (WCL) was prepared by resuspension of trypsinized cells in HEPES buffer (20 mM HEPES, protease inhibitors (Roche Applied Science), pH 7.3) prior to sonication on ice. The sonicated sample was then centrifuged (1,000 $\times$ *g* for 10 min, 4 °C), and the pellet was discarded. Subcellular fractionation of the WCL was performed by dual centrifugation steps. Supernatant from a second spin (10,000 $\times$ *g* for 20 min, 4 °C) was collected and respun (100,000 $\times$ *g* for 1 h, 4 °C) to yield supernatant (S100) and pellet (P100) fractions. The P100 pellet was washed and resuspended in HEPES buffer, prior to further sonication. For TPC overexpression experiments, SKBR3 cells were transfected (70–80% confluency) using Lipofectamine^{TM} 2000 reagent (Invitrogen) and harvested 48 h later. Fractionation of sea urchin egg homogenates was performed using the same procedures for mammalian cell lines as described above. In all cases, protein concentrations were determined by BCA assay (Thermo Scientific).

TPCN1 knock-out mice (B6;129S5-Tpcn1Gt(OST359423)Lex) were generated by Lexicon Genetics using Gene Trap by retroviral insertion of the VICTR37 vector between coding exons 1 and 2 (NM_145853). RT-PCR analysis revealed that the transcript was absent in the homozygous mutant mice. TPCN2 knock-out mice (B6;129S5-Tpcn2tm1Lex) were generated by targeted gene disruption by homologous recombination targeting coding exons 18 through 20 (NM_146206). Disruption of the target gene was confirmed by Southern hybridization analysis. Both TPCN1 and TPCN2 founder mice were backcrossed onto C57Bl6 mice for 3–4 generations before experiments. Mouse pancreatic samples were mixed with HEPES buffer (1:4, w/v) and homogenized followed by centrifugation (4,000 $\times$ *g* for 10 min, 4 °C). The supernatant was collected after further centrifugation (17,000 $\times$ *g* for 30 min, 4 °C).

Photoaffinity Labeling—Samples were incubated with [^{32}P-$5N_3$]NAADP (4.8–9.5 nM) for 5–90 min on ice prior to photoactivation effected by exposure of samples to UV light for 2 min. PAL samples were then incubated (<15 min) with SDS sample

buffer supplemented with 2-mercaptoethanol (10%) to reduce free label. SDS-PAGE was then performed by separating samples on Criterion 12.5% Bis-Tris gels (Bio-Rad) subsequently stained with instant Coomassie Brilliant Blue reagent (Invitrogen) and air-dried overnight between cellophane sheets (Sigma). For resolution of the ^{32}P signal, air-dried gels were exposed on phosphor screens (Packard Instrument Co.) at room temperature or on extra-sensitive x-ray film (Thermo Scientific) for 24–96 h at −80 °C. Quantification of ^{32}P signals was performed densitometrically using OptiQuant software (Version 3.0, Packard Instrument Co.). Curve fitting and statistical analyses were performed using GraphPad Prism (GraphPad Software Inc.). *Error bars* are shown as mean ± S.E. for each experiment. For the combined PAL/Western blotting experiment, radioactive PAL samples were separated by SDS-PAGE (4–12% Bis-Tris NuPAGE gels) and were then transferred to a nitrocellulose membrane (0.45 μm, Invitrogen) and detected with an anti-Myc antibody (1:1000, Santa Cruz Biotechnology) and an anti-mouse secondary antibody conjugated with horseradish peroxidase (1:5000, Abcam). The ^{32}P signal was exposed on x-ray film as described above.

RESULTS

The basic principle underpinning the PAL technique is summarized in Fig. 1. The radioactive photoprobe contained an azido group at the 5-carboxyl position of the nicotinic ring ($5N_3$-NAADP), and the radioactive phosphate moiety (^{32}P) was incorporated at the α position to the ribose linked to adenine (Fig. 1*A*). Azido groups are chemically inert until photoactivated by long wavelength UV light, which generates a nitrene moiety that reacts covalently with local residue(s) in the target proteins. In the absence of UV stimulation or in the presence of excess non-derivatized probe, labeling is prevented. These alternative outcomes are revealed by resolution of radioactive signal following electrophoretic separation of the PAL reaction (Fig. 1*B*).

Prior to assessment of the labeling profile of [^{32}P-$5N_3$]NAADP, it was important to ascertain the behavior of the derivatized probe ([^{32}P-$5N_3$]NAADP). Using the prototypical model for studying NAADP signaling, egg homogenates from sea urchin (*L. pictus*), specific binding of [^{32}P-$5N_3$]NAADP and [^{32}P]NAADP was dose-dependently displaced by NAADP (IC_{50} = 0.22 ± 0.05 and 0.42 ± 0.08 nM respectively, n = 6–9; Fig. 1*C*). Increasing concentrations of photoprobe ($5N_3$-NAADP) elicited progressively greater amounts of Ca^{2+} in a standard fluorometric assay (EC_{50} = 1.4 μM *versus* 32.5 nM for NAADP; Fig. 1*D*). These data demonstrate the retention of binding and Ca^{2+} release efficacy in the photoprobe. Consistent with data from another sea urchin species (*Strongylocentrotus purpuratus* (23)), homogenates subjected to the PAL reaction yielded labeling of a single, low molecular mass band (41 ± 2 kDa, n = 3; Fig. 1*E*). Labeling was completely displaced by NAADP (5 μM), but not by NADP, NAD, or nicotinic acid adenine dinucleotide (NAAD) at the same concentration (Fig. 1*E*). Selectivity for NAADP *versus* NADP was high, with little observed displacement by NADP over a wide concentration range, whereas incubation with NAADP inhibited PAL of the 41-kDa band with an IC_{50} of 0.66 ± 0.23 nM (Fig. 1, *F* and G, n = 4). Finally, comparison of the distribution of this PAL-labeled 41-kDa band (Fig. 1*H*) with the distribution of [^{32}P]NAADP binding in different membrane fractions prepared from the egg homogenate (see Fig. 1*B* in Ref. 14) showed remarkable congruence. For PAL, relative densitometry showed highest labeling in the S10P100 fraction ("light membranes"), more than 2-fold greater than P10 or P100 fractions, which closely mimicked results from [^{32}P]NAADP binding analyses (14). Therefore, the labeling characteristics of the photoaffinity probe recapitulate the basic binding, activity, and distribution characteristics of NAADP receptors in sea urchin egg homogenates.

For PAL experiments using mammalian samples, we first employed SKBR3 cells. This cell line, derived from a mammary gland adenocarcinoma, has proved to be a useful cell type for studying and manipulating endogenous NAADP-evoked Ca^{2+} signals (7). Microinjection of $5N_3$-NAADP or NAADP into single SKBR3 cells elicited a cytoplasmic Ca^{2+} signal, whereas buffer injection was without effect. These data demonstrated the efficacy of this analog in mammalian systems (Fig. 2*A*). To identify NAADP binding partners, the radioactive analog ([^{32}P-$5N_3$]NAADP) was incubated in SKBR3 whole cell lysate. After irradiation and electrophoretic separation, multiple labeled bands (Fig. 2*B*) spanning a broad molecular mass range (>20 kDa to ~250 kDa) were revealed. Not all bands labeled by [^{32}P-$5N_3$]NAADP in SKBR3 cells were affected by the presence of excess NAADP during the cross-linking reaction. For example, several bands labeled between ~30 and 70 kDa (Fig. 2*B*, *upper panel*) displayed similar labeling intensity despite the presence of NAADP. Quantification of the extent of NAADP protection was performed by densitometry using gels from multiple different samples and PAL reactions, and these results were collated in Fig. 2*B* (*lower panel*). To narrow down the list of candidates for further study, bands were prioritized that showed >2-fold reduction in ^{32}P signal intensity when the PAL reaction was performed in the presence of NAADP (10 μM). From this analysis, it was evident that four bands, at ~250 kDa (*band 1*), ~102 kDa (*band 2*), ~27 kDa (*band 8*), and a doublet at 22/23 kDa (*band 9*), met this criterion. Candidates showing poor NAADP displacement (*bands 3–7*) were not considered further.

As the most complete displacement was observed from the 22/23-kDa doublet (>4-fold, *band 9*) and a kinetic analysis of labeling implied that this candidate rapidly bound [^{32}P-$5N_3$]NAADP (Fig. 2*C*), we proceeded to assess selectivity of the 22/23-kDa doublet for NAADP relative to other ligands. To achieve this, PAL was performed in SKBR3 whole cell lysates in the presence of a variety of analogs (Fig. 2*D*). For the 22/23-kDa doublet, labeling was not protected by other nucleotide analogs (nicotinic acid; nicotinamide; NAD; NAAD; ATP; or β-nicotinamide ribose monophosphate) or Ca^{2+}-mobilizing compounds (cyclic ADP-ribose or inositol 1,4,5-trisphosphate). However, PAL signal was decreased by the presence of high concentrations of NADP (10 μM), as has been observed in prior [^{32}P]NAADP binding studies in mammalian samples (5, 26–28) as well as a cell line overexpressing TPC2 (5). In contrast, pharmacological profiling of the other candidates (*bands 1*, *2*, and *8*) were suggestive of properties divergent from those reported for the NAADP receptor: encompassing poor selectivity of NADP *versus* NAADP (*bands 1*, *2*, and *8*) and/or displace-

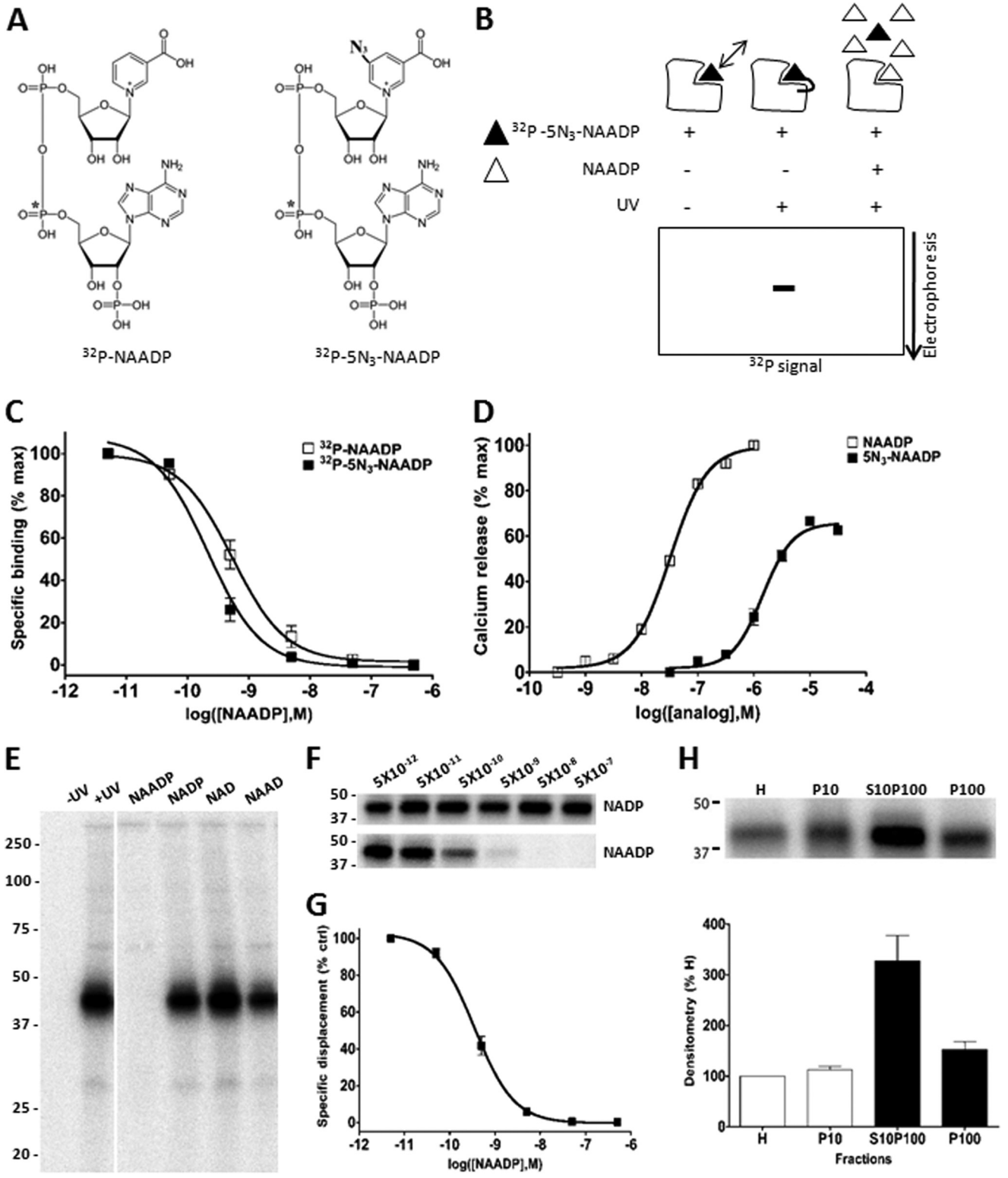

FIGURE 1. **Validation of PAL method.** *A*, chemical structure of radioactive photoprobe ([^{32}P-5N$_3$]NAADP, *right*) as compared with [^{32}P]NAADP (*left*). *B*, principle of photoaffinity labeling. In the absence of UV light, the probe reversibly binds target(s). UV exposure cross-links the radioactive photoprobe to cellular binding partner(s), which are subsequently characterized by SDS-PAGE. NAADP specificity is demonstrated by protection from labeling in the presence of excess unlabeled NAADP. *C*, displacement of [^{32}P]NAADP (*open*) and [^{32}P-5N$_3$]NAADP (*solid*) binding in *L. pictus* egg homogenates by unlabeled NAADP. *% max*, percentage of maximum. *D*, activation of Ca^{2+} release by 5N$_3$-NAADP (100 nM–31.6 μM) in *L. pictus* egg homogenates. *E*, PAL in *L. pictus* egg homogenates revealed a single band at ~41 kDa. Incubation of PAL reaction mixture with NAADP (5 μM) protected labeling, whereas other analogues (NADP, NAD, and NAAD, 5 μM) did not impact labeling. *F*, effect of the indicated concentrations of NADP (*top*) and NAADP (*bottom*) on PAL labeling of the 41-kDa band. *G*, densitometric quantification ($n = 4$) of NAADP displacement data shown in *F*. *% ctrl*, percentage of control. *H*, PAL in subcellular fractions of *L. pictus* egg homogenates. *Top*, representative PAL image in crude homogenates (*H*) and membrane fractions (*P10*, *S10P100*, and *P100*). *Bottom*, densitometric quantification of similar experiments ($n = 3$).

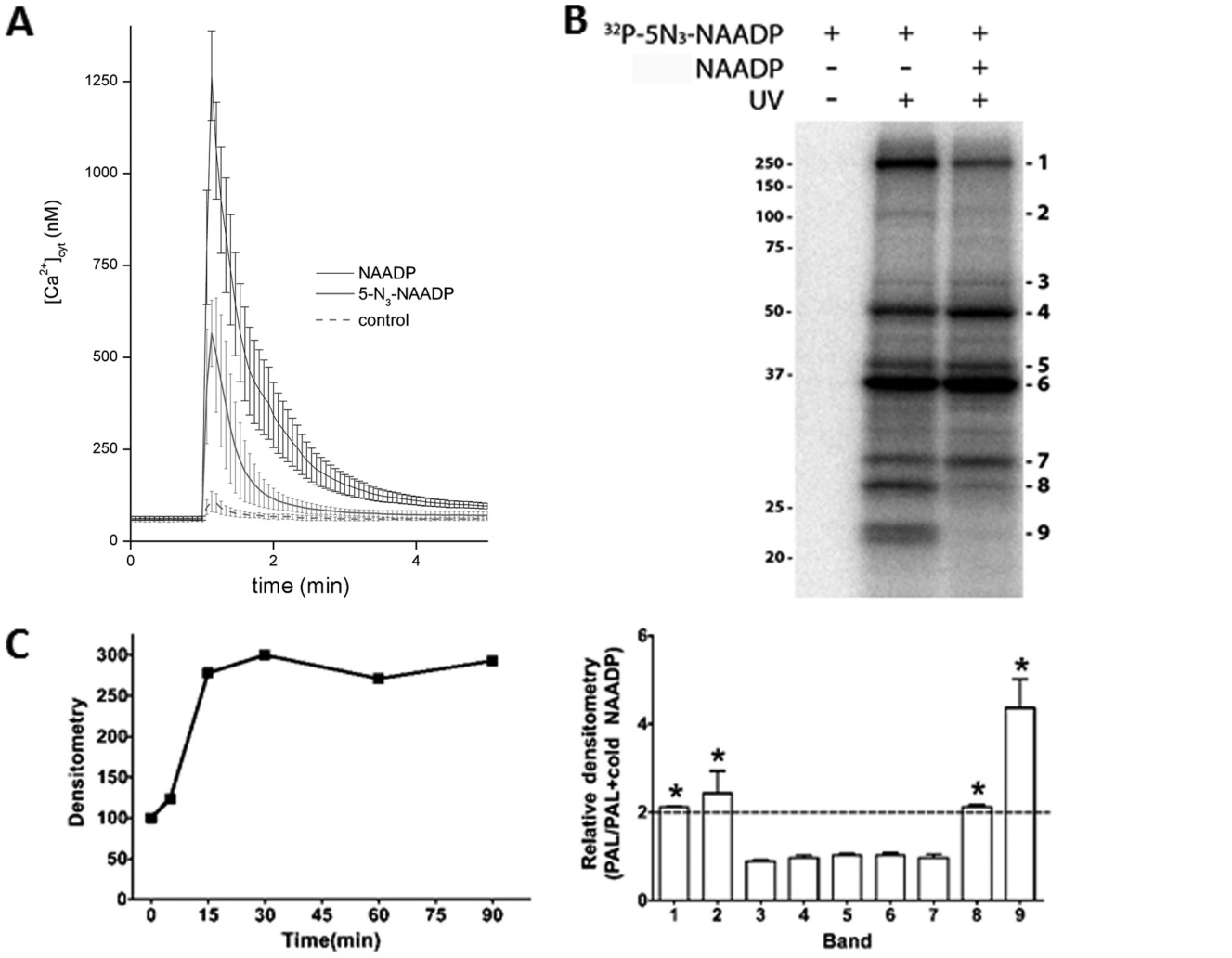
A
1250
1000
750
500
250
0
[Ca2+]cyt (nM)
NAADP
5-N3-NAADP
control
0
2
4
time (min)
B
32P-5N3-NAADP + + +
NAADP - - +
UV - + +
250
150
100
75
50
37
25
20
1
2
3
4
5
6
7
8
9
C
Densitometry
300
250
200
150
100
50
0
0 15 30 45 60 75 90
Time(min)
Relative densitometry (PAL/PAL+cold NAADP)
6
4
2
0
1 2 3 4 5 6 7 8 9
Band
D
HEPES
NAADP
NADP
5N3-NAADP
Nic. Acid
Nico.
NAD
NAAD
ATP
β-NMN
cADPR
IP3
250
150
100
75
50
37
25
20
1
2
8
9

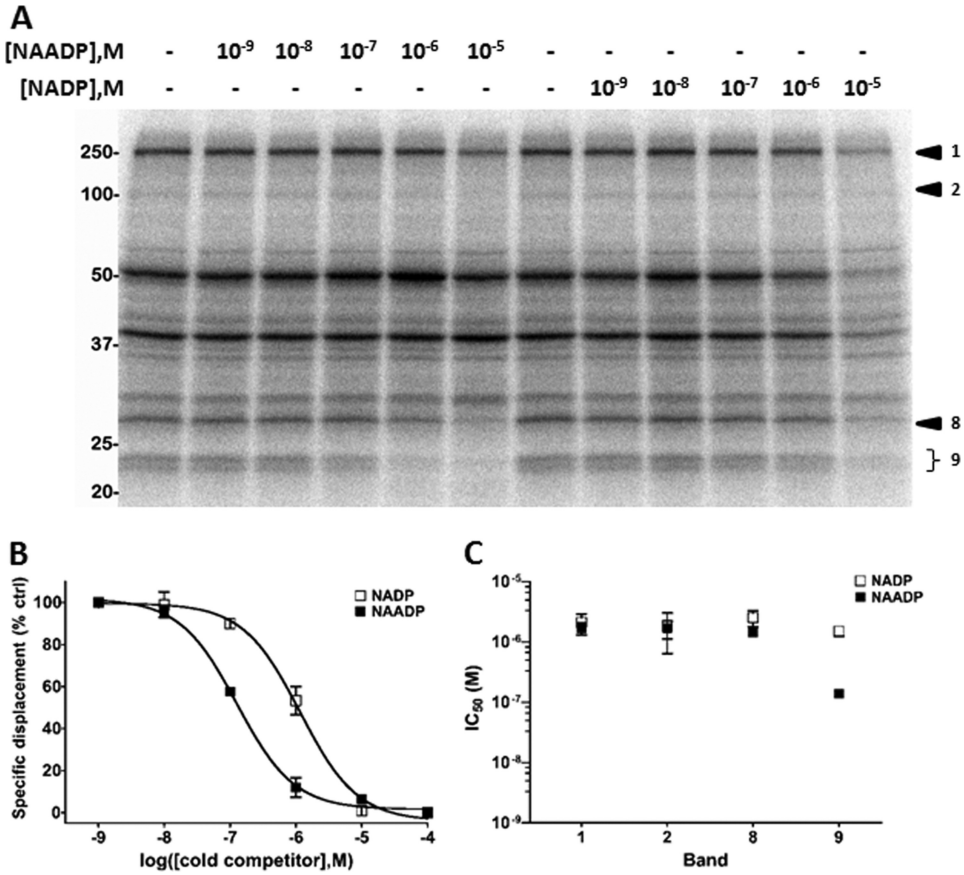

FIGURE 3. **NADP and NAADP protection of PAL in SKBR3 whole cell lysates.** *A*, representative PAL image showing effects of increasing concentrations of NAADP (*lanes 2–6*) and NADP (*lanes 8–12*) on PAL. Candidate *bands 1*, *2*, *8*, and *9* are marked. *M*, molarity. *B*, densitometry of the 22/23-kDa doublet (*band 9*, $n = 4$) from *A* in the presence of NADP (*open square*) and NAADP (*solid square*). *% ctrl*, percentage of control. *C*, comparison of half-maximal inhibitory concentrations (IC_{50}) for NADP (*open*) and NAADP (*solid*) for *bands 1*, *2*, *8*, and *9* in SKBR3 WCL ($n = 4$).

ment by other ligands (cyclic ADP-ribose, *band 8*). To better substantiate this conclusion, selectivity for NAADP *versus* NADP was examined for each of the four bands at various ligand concentrations. Fig. 3*A* shows a representative image demonstrating competition by NAADP or NADP that was used to fit competition curves. This is illustrated for the 22/23-kDa doublet (Fig. 3*B*), which displayed an IC_{50} of 137 ± 17 nM for NAADP and 1.5 ± 0.3 μM for NADP, respectively ($n = 4$; Fig. 3*B*). Comparison of IC_{50} ratios (NADP/NAADP) for each of the four candidates in SKBR3 cells underscored that only the low molecular weight doublet (*band 9*) displayed clear selectivity for NAADP over NADP (~11-fold; Fig. 3*C*).

Cellular distribution of the 22/23-kDa doublet was then assessed by subcellular fractionation. Centrifugation of whole cell lysate prior to PAL resulted in the majority (~75%) of PAL-tagged doublet (*band 9*) appearing in the supernatant (*S100*) as compared with the membrane fraction (*P100*) when the same amounts of proteins were used for PAL reaction (Fig. 4*A*). Intriguingly, competition analyses revealed that the properties of doublet-associated PAL signal differed between the supernatant (*S100*) and pellet (*P100*) fractions. PAL was inhibited by significantly lower concentrations of NAADP in the membrane fraction as compared with either S100 or WCL samples (Fig. 4*B*). Quantification of these data revealed an ~20-fold lower IC_{50} in the membrane fraction (10 ± 1 nM, $n = 3$, Fig. 4*C*) as compared with supernatant (198 ± 40 nM, $n = 3$) used in the same set of experiments. Further, selectivity of the doublet for NAADP (over NADP) was even greater in the membrane fraction (P100, ~52-fold) as compared with values measured in WCL (~11-fold) and S100 (~5-fold) samples in the same experiments (Fig. 4, *C* and *D*). Therefore, association of the doublet with membranes conferred a higher apparent NAADP binding affinity (~10 nM; ~13-fold greater than WCL) and selectivity over NADP (~52-fold; 4.5-fold greater than WCL). In summary, these data suggest that the 22/23-kDa doublet identified by PAL in SKBR3 cells displays high affinity and selectivity for NAADP (Figs. 3 and 4), as well as a similar

FIGURE 2. **Photoaffinity labeling of SKBR3 whole cell lysate.** *A*, microinjection of $5N_3$-NAADP or NAADP (both ~2 μM final) but not buffer alone (*control*) increases intracellular Ca^{2+} in SKBR3 cells. *B*, *top*, representative PAL image in WCL of SKBR3 cells. In the presence of UV light, the intensity of nine bands (~20–250 kDa, *bands 1–9*) was quantified in the absence (*lane 2*) and presence (*lane 3*) of excess NAADP. *Bottom*, quantification of protection of labeling by NAADP, expressed as ratio of PAL intensities (absence/presence of NAADP). Four candidates (*) with estimated molecular masses of ~250 kDa (*band 1*), 102 kDa (*band 2*), 27 kDa (*band 8*), and a 23-kDa doublet (*band 9*) displayed ≥2-fold displacement by NAADP (10 μM, $n = 4$). *C*, photolabeling kinetics of the 22/23-kDa doublet (*band 9*) as assessed by densitometry. *D*, effects of other compounds (all at 10 μM) on PAL in SKBR3. *Bands 1*, *2*, *8*, and *9* identified in *A* are highlighted. *Nic. Acid*, nicotinic acid; *Nico.*, nicotinamide; *β-NMN*, β-nicotinamide ribose monophosphate; *cADPR*, cyclic ADP-ribose; *IP3*, inositol 1,4,5-trisphosphate.

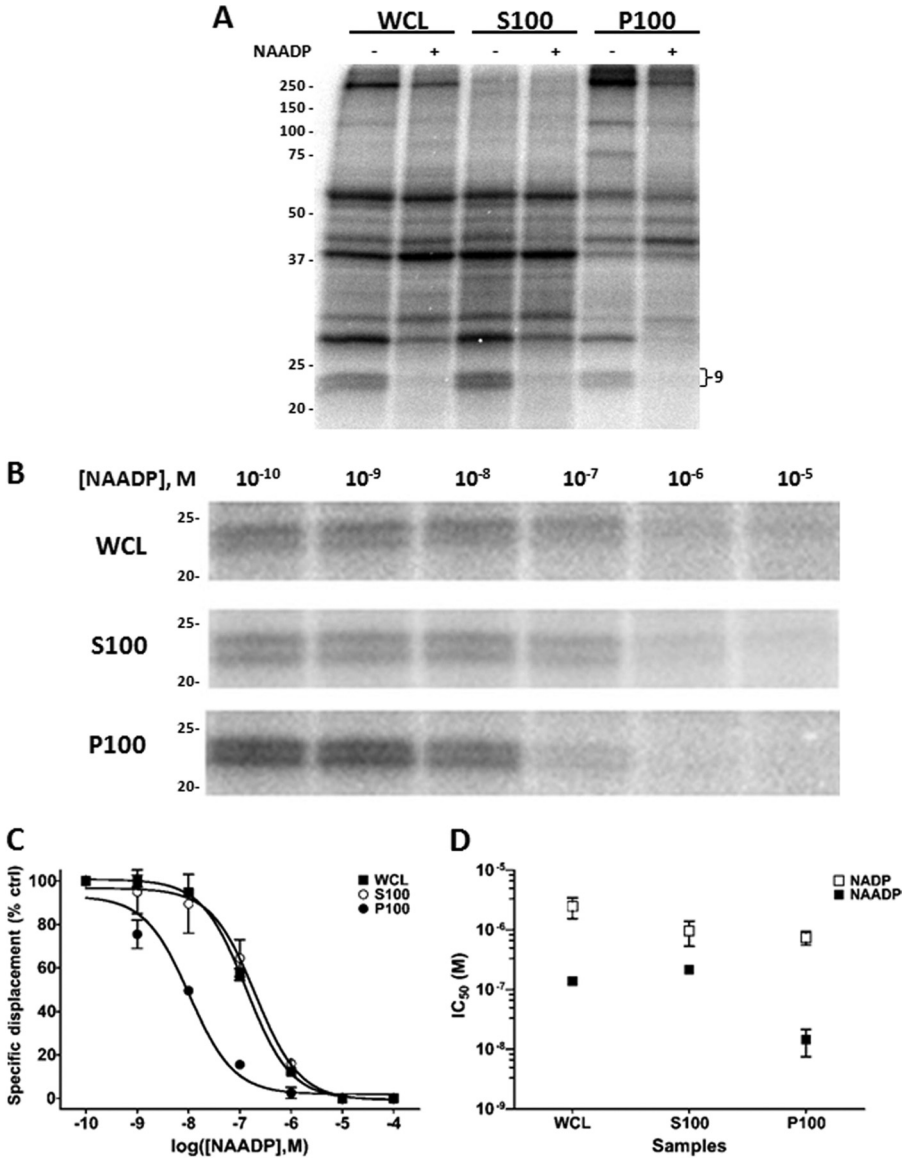

FIGURE 4. **Properties of the 23-kDa doublet in different SKBR3 subcellular fractions.** *A*, representative PAL image comparing SKBR3 WCL, soluble (*S100*), and membrane fractions (*P100*). *B*, competition PAL images of the 23-kDa doublet (*band 9*) in indicated fractions. Higher amounts of protein were loaded for the P100 fraction to facilitate visualization of the 22/23-kDa doublet. *M*, molarity. *C*, densitometry ($n = 4$) of the 22/23-kDa doublet (*band 9*) from WCL (*squares*), S100 (*open circles*), and P100 (*filled circles*) fractions. *% ctrl*, percentage of control. *D*, comparison of IC_{50} values for NADP (*open*) and NAADP (*solid*) for *band 9* in different fractions isolated from SKBR3 cells ($n = 4$).

pharmacological displacement profile to that observed for NAADP-sensitive Ca^{2+} release (Fig. 2*D*).

Next, we proceeded to apply the PAL approach in two other cell types, HEK293 cells and mouse pancreas. Both systems have been used as models for studying NAADP-evoked Ca^{2+} signals (5, 6, 9, 10, 14, 29, 30). PAL samples from HEK WCL displayed a broadly similar labeling pattern to those observed from SKBR3 cells (Fig. 5*A*). The same nomenclature (*bands 1–9*) was therefore used for similar sized bands, and additional PAL targets resolved in HEK293 cells were assigned in sequence (*bands 10–12*). Analysis of NAADP displacement yielded six candidate bands with displacement ≥2-fold (Fig. 5*B*). Four of these corresponded to those in SKBR3 cells (*bands 1*, *2*, *8*, and *9*), and two were novel (*bands 11* and *12*). Competition curves comparing labeling in the presence of varying concentrations of NAADP and NADP were then performed for all these candidates, and the quantified data ($n = 3$ independent experiments) are shown in Fig. 5*C*. These data revealed that the highest affinity and highest selectivity for NAADP were again associated with *band 9* (22/23 kDa, IC_{50} for NAADP = 52 ± 2 nM, *versus* 818 ± 106 nM for NADP using WCL, $n = 3$). Moreover, similar to data from SKBR3 cells (Fig. 4*C*), IC_{50} values in membrane (P100) fractions from HEK cells were indicative of a higher apparent affinity of the 23-kDa candidate when membrane-associated (IC_{50} for NAADP = 22 ± 4 nM *versus* 134 ± 23 nM in P100 *versus* S100 fractions, respectively, $n = 3$).

As mouse pancreatic acinar cells have been widely used to study endogenous NAADP-evoked Ca^{2+} signaling (29, 30), we performed PAL in homogenized samples from mouse pancreas. NAADP displacement identified six candidates at low molecular masses (<50 kDa) in the pancreatic samples with little obvious labeling of larger proteins (Fig. 5*D*). As this labeling pattern

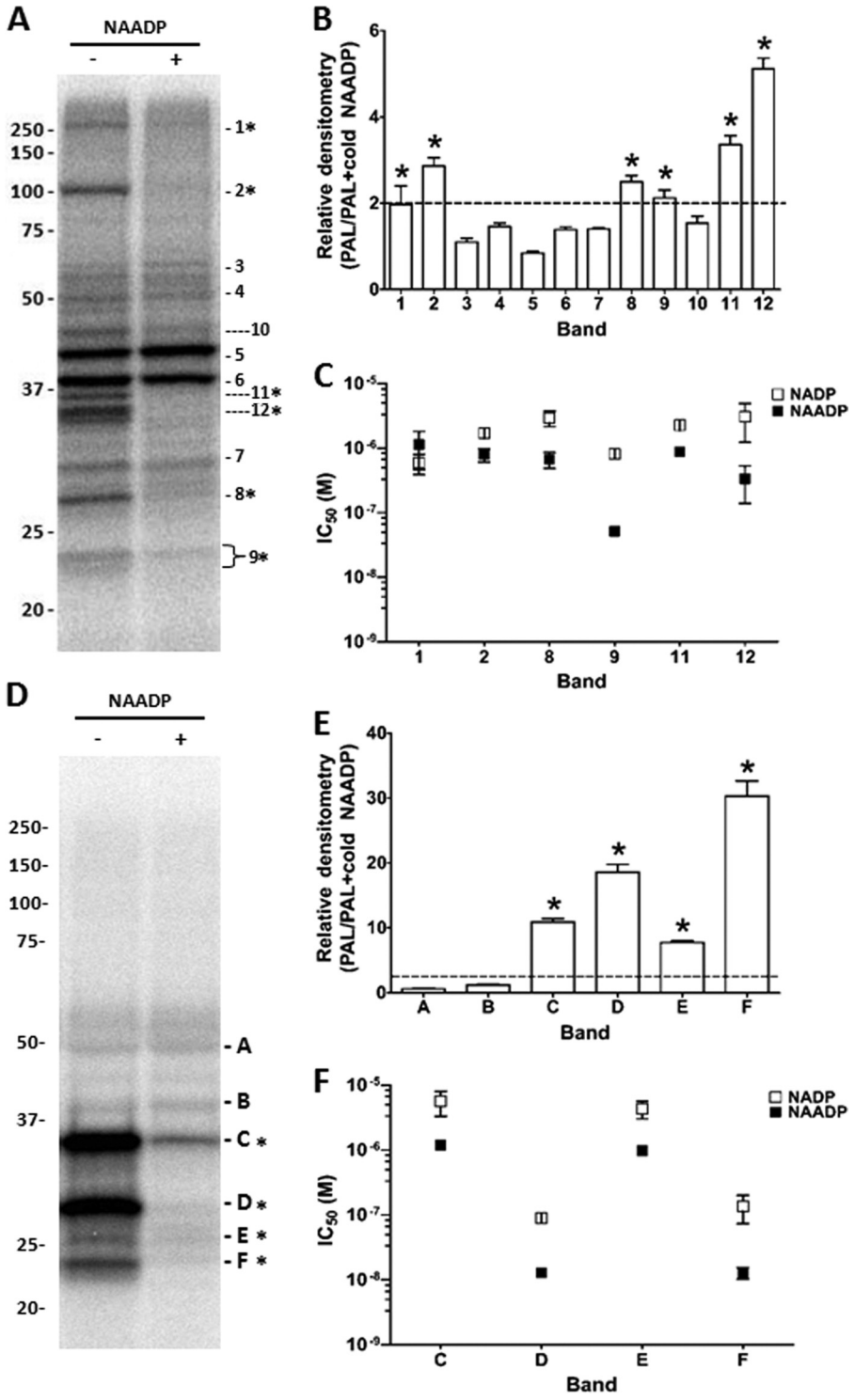

FIGURE 5. **PAL in HEK293 cells and mouse pancreas.** *A*, representative PAL gel in HEK293 WCL. Band numbering was kept consistent with similar sized bands observed in SKBR3 cells. *B*, ratio of densitometry of the indicated bands (*bands 1–12*) from multiple independent experiments. Six candidates (*) with estimated molecular masses ~250 kDa (*band 1*), 102 kDa (*band 2*), 27 kDa (*band 8*), 23-kDa doublet (*band 9*), 36 kDa (*band 11*), and 35 kDa (*band 12*) displayed ≥2-fold displacement by NAADP (10 μM, $n = 4$). *C*, measurements of IC_{50} values for bands that displayed >2-fold protection by NAADP. *D–F*, similar processing for mouse pancreatic samples (Pel-Freez Biologicals) showing representative gel (*D*), NAADP displacement ratio (*E*), and IC_{50} estimation (*F*).

was different from that observed in human cell lines, we employed a different nomenclature for the pancreatic candidates (*bands A–F*). Quantification of displacement by NAADP revealed that four PAL bands showed significant protection by NAADP, well in excess of the 2-fold criterion established in either human cell line (*bands C–F*, ~6–30-fold displacement). Assessment of the selectivity for NAADP over NADP revealed that *band F* (23 kDa) and *band D* (27 kDa) displayed the highest selectivity for NAADP over NADP (9.3 ± 2.3- and 7.6 ± 1.8-fold for *bands F* and *D* respectively, $n = 4$; Fig. 5*F*). Therefore, in

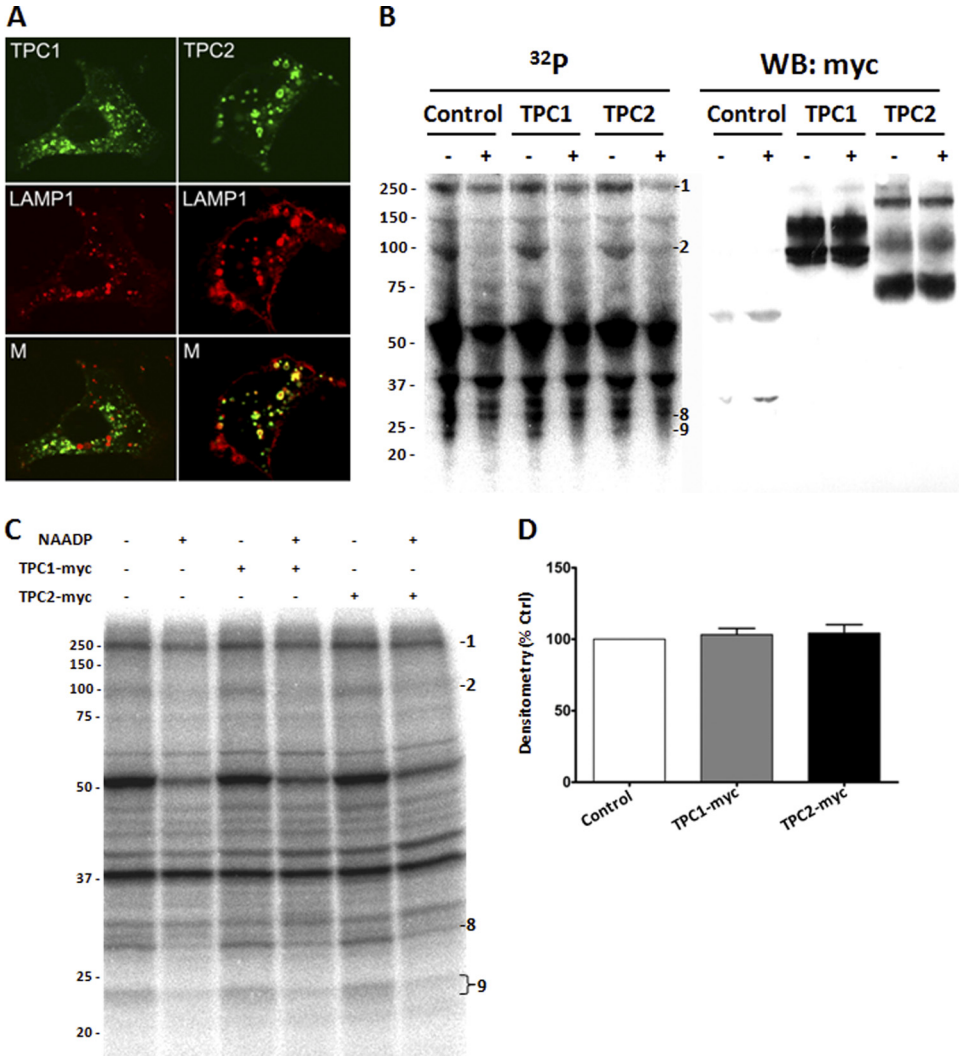

FIGURE 6. **Lack of effect of overexpressed TPC isoforms on PAL profiles.** *A*, images of SKBR3 cells transfected with TPC1-GFP (*upper left*) or TPC2-GFP (*upper right*) and in live cells co-expressing LAMP1-RFP (*middle panel*). *Bottom*, merged images for GFP and RFP. *B*, combined PAL/Western blot, allowing comparison of PAL reactivity (*left*) with immunological detection of TPC isoforms (*right*) on the same nitrocellulose membrane. Control cells were transfected with a Myc-GFP construct. *WB*, Western blot. *C*, representative PAL gel comparing reactivity in control WCL (transfected with Myc-ER) with TPC1-Myc (*middle two lanes*) and TPC2-Myc (*right two lanes*) transfected cells. Overexpression of TPC isoforms did not impact the PAL labeling profile in the absence or presence of NAADP. *D*, quantification of levels of the 22/23-kDa doublet in TPC1-Myc and TPC2-Myc transfected SKBR3 cells relative to controls ($n = 4$ independent transfections). *% Ctrl*, percentage of control.

each of three different mammalian samples studied (SKBR3, HEK293, and mouse pancreas), the 22/23-kDa doublet consistently displayed the highest apparent affinity and selectivity for NAADP.

The sizes of the NAADP-selective candidates (22 and 23 kDa) in mammalian cells and the single 41-kDa band in sea urchin (*L. pictus*) were considerably lower than those expected for the TPC proteins identified as NAADP-sensitive Ca^{2+} channels (9, 13, 31). Two possible explanations for this discrepancy are that (i) endogenous levels of TPCs are below the detection capability of the PAL approach or (ii) the low molecular weight candidates are actually degradation products of the full-length TPC protein. These possibilities were discounted by examining the effects of TPC overexpression, which is a straightforward assay in the mammalian (but not sea urchin) system. Given that the sensitivity of detection of Western blot methods is lower than that of ^{32}P-based PAL methods (typically pico- *versus* femtogram sensitivity), immunological detection of overexpressed TPCs should obviate concerns of whether an insufficient amount of TPC existed in the PAL samples and whether the full-length protein was present. Further, increased levels of TPC should cause an increase in PAL reactivity if NAADP is binding directly to these channels.

Therefore, we overexpressed GFP-tagged human TPC1 and TPC2 in SKBR3 cells. Both constructs were observed to target to intracellular structures (Fig. 6*A*). These data confirm previous reports that TPC constructs are faithfully targeted in the SKBR3 system (7). Next, we expressed Myc-tagged TPC1 and TPC2 constructs with a view to performing Western blotting and phosphorimaging on the same set of PAL samples separated on an SDS-PAGE gel and transferred to a single membrane. The resulting PAL reaction (lower resolution because of membrane transfer) and Western blot are shown in Fig. 6*B*. These data revealed that TPC reactivity was localized as expected at sizes consistent with full-length/glycosylated TPC1 (~93 and 130 kDa) and TPC2 (~69, 107, and 229 kDa) and

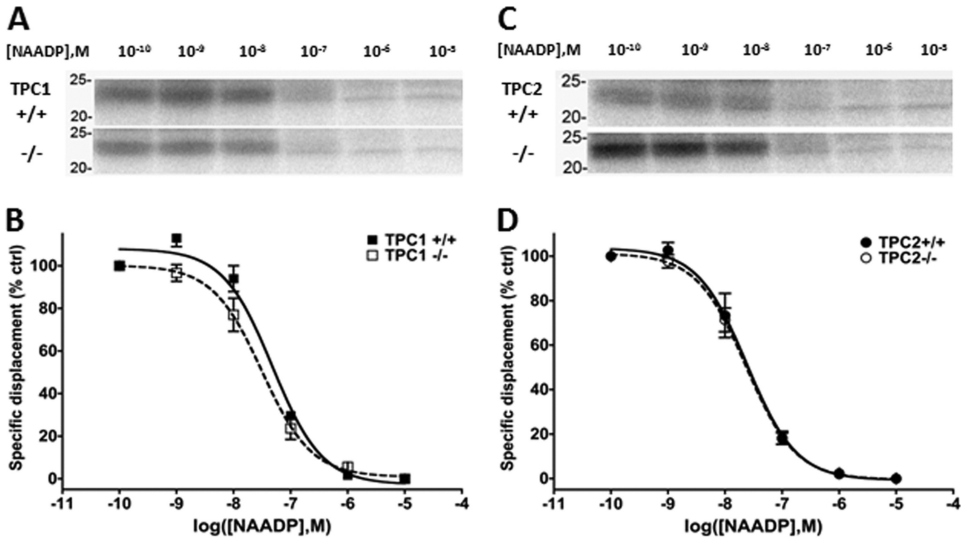

FIGURE 7. **PAL in TPC knock-out mouse pancreas.** *A* and *C*, PAL profile for the 22/23-kDa doublet compared between TPC1$^{+/+}$ *versus* TPC1$^{-/-}$ (*A*) and TPC2$^{+/+}$ *versus* TPC2$^{-/-}$ (*C*) WCL samples. *M*, molarity. *B* and *D*, quantification of IC_{50} values in similar samples ($n = 3$) shown in *A* and *C*. *% ctrl*, percentage of control.

control Myc-ER samples at <30 kDa. However, overexpression of TPCs did not change the overall PAL labeling pattern and specifically the intensity of the 22/23-kDa bands. Comparison of the PAL and Western blot data confirm that although full-length TPC1 and TPC2 are clearly detectable in these samples, their migration does not correlate well with the 22/23-kDa doublet.

PAL of the same TPC overexpressed samples was then performed at higher resolution to allow densitometric quantification (Fig. 6*C*). Again, overexpression of Myc-tagged TPC1 or TPC2 resulted in very similar PAL patterns, with no obvious appearance of novel candidates within the size range expected for these channels in either the presence or the absence of NAADP. Further, PAL did not change the migration pattern of TPCs, as judged by comparison with non-irradiated samples (data not shown). Densitometry of the 22/23-kDa doublet in the overexpressed samples showed no increase in both TPC1-Myc (103 ± 4%, $n = 4$) and TPC2-Myc (104 ± 6%, $n = 4$) whole cell lysates as compared with mock transfection (Fig. 6*D*). Given that the PAL approach has higher sensitivity than Western blotting, it is unlikely that the failure to demonstrate labeling of TPCs results from insufficient TPC levels in these samples. Rather, we conclude that labeling with [^{32}P-5N$_3$]NAADP does not correlate with TPC immunoreactivity in samples where the presence of full-length TPC proteins is readily demonstrable.

Finally, we examined PAL patterns in pancreatic samples derived from TPCN1 and TPCN2 knock-out mice. The availability of these samples afforded the opportunity to examine PAL labeling patterns following ablation of endogenous TPC isoforms. Interestingly, the 22/23-kDa doublet was present in all the different pancreatic samples (Fig. 7) despite the targeting of TPC isoforms for ablation (TPC1$^{+/+}$ matched littermate *versus* TPC1$^{-/-}$; TPC2$^{+/+}$ *versus* TPC2$^{-/-}$). Further, the IC_{50} values for displacement of PAL reactivity by unlabeled NAADP were similar for TPC1 (IC_{50} for NAADP of 48 ± 3 nM TPC1$^{+/+}$ *versus* 33 ± 9 nM TPC1$^{-/-}$; Fig. 7, *A* and *B*) and TPC2 knock-out samples (IC_{50} for NAADP of 26 ± 8 nM TPC2$^{+/+}$ *versus* 24 ± 5 nM TPC2$^{-/-}$; Fig. 7, *C* and D). These data demonstrate that the 22/23-kDa NAADP-selective doublet is present in TPC knock-out samples and therefore represents a unique protein distinct from either TPC isoform.

DISCUSSION

The two-pore channels (TPC1 and TPC2 in humans) have recently been identified as a family of endolysosomal ion channels that release Ca^{2+} from acidic organelles in response to NAADP (5–7). However, there is currently no insight as to how NAADP activates these channels at the structural level. Therefore, the original rationale for this work was to utilize a photolabeling method to identify which region(s) of the TPC protein bind to NAADP, guided by similar studies that have successfully mapped regions/residues that coordinate ligand-ion channel interactions (19–21). However, rather than labeling candidates with sizes equivalent to TPC1/2, results from all the systems examined in this study converged in identifying a lower molecular mass candidate (22/23-kDa bands in mammalian systems) as an NAADP target that displayed characteristics compatible with NAADP-evoked Ca^{2+} release. In each of the three mammalian systems examined, this labeled doublet displayed: (i) the highest affinity for NAADP, (ii) the greatest selectivity for NAADP over NADP, and (iii) a minority fraction of total PAL labeling as expected for a receptor (properties summarized in Table 1). In SKBR3 cells, the pharmacology of this candidate mimicked known properties of NAADP-sensitive Ca^{2+} release and showed the highest degree of protection by NAADP of any labeled proteins (Fig. 2). Further selectivity for NAADP over NADP was ~52-fold in the SKBR3 membrane fraction (Fig. 4), a ratio that compared favorably with published selectivity ratios from [^{32}P]NAADP binding assays (*e.g.* 7–49-fold range (26–28)), which are taken as representative of the NAADP-evoked Ca^{2+} release mechanism. Finally, comparison of PAL results between the three mammalian samples (Table 1) revealed that the low molecular weight doublet comprised a

TABLE 1

Photolabeling characteristics of 22/23-kDa doublet in three different mammalian samples

Comparison of PAL reactivity in WCL samples between the two human cell lines and mouse pancreas was performed in terms of (i) fraction of total sample labeling (left column), (ii) extent of protection by NAADP (10 μM, middle column), and (iii) selectivity of labeling (IC_{50}(NADP)/IC_{50}(NAADP), right column).

	Doublet labeling (% of total)	Inhibition by NAADP	Selectivity over NADP
HEK293	3 ± 0.2%	2 ± 0.2-fold	~15-fold
SKBR3	6 ± 0.4%	4 ± 0.7-fold	~10-fold
Mouse pancreas	10 ± 0.6%	30 ± 2.3 -fold	~8-fold

greater fraction of total labeling and exhibited greater protection by NAADP in mouse pancreatic samples. This correlates with the frequent usage of this system for studying endogenous NAADP-evoked Ca^{2+} signals as compared with cell lines where responses to microinjected NAADP are less easily demonstrated. Therefore, the failure to demonstrate labeling of endogenous TPC proteins in different mammalian or sea urchin samples, even when TPC1 and TPC2 isoforms were overexpressed, and the similarity of labeling profile in knockout samples were surprising and merit critical reevaluation of: (i) the photoaffinity approach itself and (ii) the issue of whether NAADP-evoked Ca^{2+} release occurs via TPC directly, or rather, by binding accessory proteins within a larger TPC-containing complex.

First, although the photolabeling approach provided an unbiased sampling of cellular binding partners for NAADP, results must be interpreted cautiously. Methodological concerns include the specificity of the modified photoprobe relative to the endogenous ligand, the propensity for nonspecific incorporation, and preferential labeling of low-affinity, high capacity sites. In our hands, specificity of the photoprobe was demonstrated by high affinity binding and efficacy in sea urchin egg homogenate and SKBR3 cells. Further, the observed characteristics of doublet labeling (minority fraction of total incorporation, high affinity and extent of protection, appropriate pharmacology) are not consistent with those expected for a low affinity, nonspecific site. Target abundance issues also seem unlikely given that overexpression of TPC isoforms did not result in the appearance of a size-matched PAL band despite evident immunoreactivity.

How inconsistent is this suggestion with published findings regarding NAADP binding to TPC proteins? Calcraft *et al.* (5) reported that TPC2 overexpression in HEK293 cells enhanced specific [^{32}P]NAADP binding (5). However, it was noted that conditions that resulted in a >250-fold increase in TPC2 mRNA conferred only an ~3-fold increase in specific [^{32}P]NAADP binding (5). Subsequent immunoprecipitation studies demonstrated that pulldown of sea urchin TPCs recovered [^{32}P]NAADP binding sites (14), but neither the efficiency of recovery nor the purity of the preparation was assessed. Similarly, the potential association of accessory proteins in electrophysiological assessments of TPC function cannot be excluded (9, 11, 12). Therefore, in our opinion, currently published data do not exclude the possibility that the NAADP receptor and NAADP-gated channel (TPC) are separate molecular entities such that NAADP binds to an accessory protein within a larger TPC complex. Indeed, TPCs display sequence similarity to voltage-sensitive calcium and sodium channels that assemble as multiprotein complexes encompassing tightly associated subunits (3). Discrimination of these alternatives would be facilitated by either direct demonstration of [^{32}P]NAADP binding to purified TPC proteins (no mapping of NAADP binding site(s) on the TPC channels have yet been reported) or the identification of alternate NAADP binding partners (with subsequent proof of interaction with TPCs and conferral of NAADP binding ability). In this regard, we note the compatibility of photoaffinity labeling tools with mass spectrometry methods as a logical strategy for future identification and evaluation of the relationship between the mammalian and sea urchin candidates. However, such an approach will necessitate the development of a bifunctional PAL probe (17, 32) based on low endogenous levels of this candidate in all mammalian systems examined to date.

In conclusion, our data imply the existence of an NAADP-binding protein displaying properties diagnostic of the NAADP-evoked Ca^{2+} release mechanism but which is distinct from the TPC.

REFERENCES

1. Lee, H. C. (2005) Nicotinic acid adenine dinucleotide phosphate (NAADP)-mediated calcium signaling. *J. Biol. Chem.* **280,** 33693–33696
2. Galione, A., Morgan, A. J., Arredouani, A., Davis, L. C., Rietdorf, K., Ruas, M., and Parrington, J. (2010) NAADP as an intracellular messenger regulating lysosomal calcium release channels. *Biochem. Soc. Trans.* **38,** 1424–1431
3. Hooper, R., and Patel, S. (2012) in *Calcium Signaling, Advances in Experimental Medicine and Biology* (Islam, M. S., ed), Vol. 740, Springer-Verlag New York Inc., New York, in press
4. Galione, A., Parrington, J., and Funnell, T. (2011) Physiological roles of NAADP-mediated Ca^{2+} signaling. *Sci. China Life Sci.* **54,** 725–732
5. Calcraft, P. J., Ruas, M., Pan, Z., Cheng, X., Arredouani, A., Hao, X., Tang, J., Rietdorf, K., Teboul, L., Chuang, K. T., Lin, P., Xiao, R., Wang, C., Zhu, Y., Lin, Y., Wyatt, C. N., Parrington, J., Ma, J., Evans, A. M., Galione, A., and Zhu M. X. (2009) NAADP mobilizes calcium from acidic organelles through two-pore channels. *Nature* **459,** 596–600
6. Zong, X., Schieder, M., Cuny, H., Fenske, S., Gruner, C., Rötzer, K., Griesbeck, O., Harz, H., Biel, M., and Wahl-Schott, C. (2009) The two-pore channel TPCN2 mediates NAADP-dependent Ca^{2+} release from lysosomal stores. *Pflugers Arch.* **458,** 891–899
7. Brailoiu, E., Churamani, D., Cai, X., Schrlau, M. G., Brailoiu, G. C., Gao, X., Hooper, R., Boulware, M. J., Dun, N. J., Marchant, J. S., and Patel, S. (2009) Essential requirement for two-pore channel 1 in NAADP-mediated calcium signaling. *J. Cell Biol.* **186,** 201–209
8. Dionisio, N., Albarrán, L., López, J. J., Berna-Erro, A., Salido, G. M., Bobe, R., and Rosado, J. A. (2011) Acidic NAADP-releasable Ca^{2+} compartments in the megakaryoblastic cell line MEG01. *Biochim. Biophys. Acta* **1813,** 1483–1494
9. Brailoiu, E., Rahman, T., Churamani, D., Prole, D. L., Brailoiu, G. C., Hooper, R., Taylor, C. W., and Patel, S. (2010) An NAADP-gated two-pore channel targeted to the plasma membrane uncouples triggering from amplifying Ca^{2+} signals. *J. Biol. Chem.* **285,** 38511–38516
10. Ogunbayo, O. A., Zhu, Y., Rossi, D., Sorrentino, V., Ma, J., Zhu, M. X., and Evans, A. M. (2011) Cyclic adenosine diphosphate ribose activates ryanodine receptors, whereas NAADP activates two-pore domain channels. *J. Biol. Chem.* **286,** 9136–9140

11. Schieder, M., Rötzer, K., Brüggemann, A., Biel, M., and Wahl-Schott, C. A. (2010) Characterization of two-pore channel 2 (TPCN2)-mediated Ca^{2+} currents in isolated lysosomes. *J. Biol. Chem.* **285,** 21219–21222
12. Pitt, S. J., Funnell, T. M., Sitsapesan, M., Venturi, E., Rietdorf, K., Ruas, M., Ganesan, A., Gosain, R., Churchill, G. C., Zhu, M. X., Parrington, J., Galione, A., and Sitsapesan, R. (2010) TPC2 is a novel NAADP-sensitive Ca^{2+} release channel, operating as a dual sensor of luminal pH and Ca^{2+}. *J. Biol. Chem.* **285,** 35039–35046
13. Yamaguchi, S., Jha, A., Li, Q., Soyombo, A. A., Dickinson, G. D., Churamani, D., Brailoiu, E., Patel, S., and Muallem, S. (2011) Transient receptor potential mucolipin 1 (TRPML1) and two-pore channels are functionally independent organellar ion channels. *J. Biol. Chem.* **286,** 22934–22942
14. Ruas, M., Rietdorf, K., Arredouani, A., Davis, L. C., Lloyd-Evans, E., Koegel, H., Funnell, T. M., Morgan, A. J., Ward, J. A., Watanabe, K., Cheng, X., Churchill, G. C., Zhu, M. X., Platt, F. M., Wessel, G. M., Parrington, J., and Galione, A. (2010) Purified TPC isoforms form NAADP receptors with distinct roles for Ca^{2+} signaling and endolysosomal trafficking. *Curr. Biol.* **20,** 703–709
15. Dormán, G., and Prestwich, G. D. (2000) Using photolabile ligands in drug discovery and development. *Trends Biotechnol.* **18,** 64–77
16. Weber, P. J., and Beck-Sickinger, A. G. (1997) Comparison of the photochemical behavior of four different photoactivatable probes. *J. Pept. Res.* **49,** 375–383
17. Lamos, S. M., Krusemark, C. J., McGee, C. J., Scalf, M., Smith, L. M., and Belshaw, P. J. (2006) Mixed isotope photoaffinity reagents for identification of small-molecule targets by mass spectrometry. *Angew. Chem. Int. Ed. Engl.* **45,** 4329–4333
18. Jain, P., Slama, J. T., Perez-Haddock, L. A., and Walseth, T. F. (2010) Nicotinic acid adenine dinucleotide phosphate analogues containing substituted nicotinic acid: effect of modification on Ca^{2+} release. *J. Med. Chem.* **53,** 7599–7612
19. Tomizawa, M., Maltby, D., Medzihradszky, K. F., Zhang, N., Durkin, K. A., Presley, J., Talley, T. T., Taylor, P., Burlingame, A. L., and Casida, J. E. (2007) Defining nicotinic agonist binding surfaces through photoaffinity labeling. *Biochemistry* **46,** 8798–8806
20. Tomizawa, M., Talley, T. T., Park, J. F., Maltby, D., Medzihradszky, K. F., Durkin, K. A., Cornejo-Bravo, J. M., Burlingame, A. L., Casida, J. E., and Taylor, P. (2009) Nicotinic agonist binding site mapped by methionine- and tyrosine-scanning coupled with azidochloropyridinyl photoaffinity labeling. *J. Med. Chem.* **52,** 3735–3741
21. Tanabe, K., Tucker, S. J., Matsuo, M., Proks, P., Ashcroft, F. M., Seino, S., Amachi, T., and Ueda, K. (1999) Direct photoaffinity labeling of the Kir6.2 subunit of the ATP-sensitive K+ channel by 8-azido-ATP. *J. Biol. Chem.* **274,** 3931–3933
22. Aarhus, R., Graeff, R. M., Dickey, D. M., Walseth, T. F., and Lee, H. C. (1995) ADP-ribosyl cyclase and CD38 catalyze the synthesis of a calcium-mobilizing metabolite from NADP. *J. Biol. Chem.* **270,** 30327–30333
23. Walseth, T. F., Lin-Moshier, Y., Jain, P., Ruas, M., Parrington, J., Galione, A., Marchant, J. S., and Slama, J. T. (2012) Photoaffinity labeling of high affinity nicotinic acid adenine dinucleotide phosphate (NAADP)-binding proteins in sea urchin egg. *J. Biol. Chem.* **287,** 2308–2315
24. Lee, H. C., Aarhus, R., and Walseth, T. F. (1993) Calcium mobilization by dual receptors during fertilization of sea urchin eggs. *Science* **261,** 352–355
25. Genazzani, A. A., Empson, R. M., and Galione, A. (1996) Unique inactivation properties of NAADP-sensitive Ca^{2+} release. *J. Biol. Chem.* **271,** 11599–11602
26. Gambara, G., Billington, R. A., Debidda, M., D'Alessio, A., Palombi, F., Ziparo, E., Genazzani, A. A., and Filippini, A. (2008) NAADP-induced Ca^{2+} signaling in response to endothelin is via the receptor subtype B and requires the integrity of lipid rafts/caveolae. *J. Cell Physiol.* **216,** 396–404
27. Bak, J., Billington, R. A., Timar, G., Dutton, A. C., and Genazzani, A. A. (2001) NAADP receptors are present and functional in the heart. *Curr. Biol.* **11,** 987–990
28. Billington, R. A., Bellomo, E. A., Floriddia, E. M., Erriquez, J., Distasi, C., and Genazzani, A. A. (2006) A transport mechanism for NAADP in a rat basophilic cell line. *FASEB J.* **20,** 521–523
29. Cancela, J. M., Churchill, G. C., and Galione, A. (1999) Coordination of agonist-induced Ca^{2+}-signalling patterns by NAADP in pancreatic acinar cells. *Nature* **398,** 74–76
30. Cancela, J. M., Gerasimenko, O. V., Gerasimenko, J. V., Tepikin, A. V., and Petersen, O. H. (2000) Two different but converging messenger pathways to intracellular Ca^{2+} release: the roles of nicotinic acid adenine dinucleotide phosphate, cyclic ADP-ribose, and inositol trisphosphate. *EMBO J.* **19,** 2549–2557
31. Hooper, R., Churamani, D., Brailoiu, E., Taylor, C. W., and Patel, S. (2011) Membrane topology of NAADP-sensitive two-pore channels and their regulation by *N*-linked glycosylation. *J. Biol. Chem.* **286,** 9141–9149
32. Robinette, D., Neamati, N., Tomer, K. B., and Borchers, C. H. (2006) Photoaffinity labeling combined with mass spectrometric approaches as a tool for structural proteomics. *Expert Rev. Proteomics* **3,** 399–408